Acta Neurol Scand DOI: 10.1111/j.1600-0404.2008.01053.x

Copyright © 2008 The Authors
Journal compilation © 2008 Blackwell Munksgaard

ACTA NEUROLOGICA
SCANDINAVICA

Decreased dopamine D_2 receptor binding in essential blepharospasm

Horie C, Suzuki Y, Kiyosawa M, Mochizuki M, Wakakura M, Oda K, Ishiwata K, Ishii K. Decreased dopamine D_2 receptor binding in essential blepharospasm.
Acta Neurol Scand: DOI: 10.1111/j.1600-0404.2008.01053.x.
© 2008 The Authors Journal compilation © 2008 Blackwell Munksgaard.

Objectives – The purpose of this study was to investigate whether dopamine D_2 receptor binding was altered in the striatum of essential blepharospasm patients. *Methods* – Striatal dopamine D_2 receptor binding was measured with positron emission tomography and [^{11}C]raclopride. We studied eight drug-naive patients with bilateral blepharospasm and eight age-matched normal controls. *Results* – The uptake indices in the blepharospasm group were significantly reduced by 11.7% in the caudate ($P < 0.005$), 11.6% in the anterior putamen ($P < 0.0001$), and 10.3% in the posterior putamen ($P < 0.005$) relative to the control group. *Conclusions* – This study indicates decreased dopamine D_2 receptor binding in the entire striatal region of blepharospasm patients. The findings suggest that decreased dopamine D_2 receptor binding might be one of the predisposing factors that leads to the dysfunction of the motor circuit, resulting in the loss of broad inhibition of unwanted movements during an intended movement in blepharospasm patients.

C. Horie[1,2], Y. Suzuki[1,2], M. Kiyosawa[1], M. Mochizuki[1], M. Wakakura[3], K. Oda[2], K. Ishiwata[2], K. Ishii[2]

[1]Department of Ophthalmology and Visual Science, Tokyo Medical and Dental University Graduate School, Tokyo, Japan; [2]Positron Medical Center, Tokyo Metropolitan Institute of Gerontology, Tokyo, Japan; [3]Inouye Eye Hospital, Tokyo, Japan

Key words: dopamine D_2 receptor; essential blepharospasm; positron emission tomography; [^{11}C]raclopride

Kenji Ishii, Positron Medical Center, Tokyo Metropolitan Institute of Gerontology, 1-1 Naka-cho, Itabashi-ku, Tokyo 173-0022, Japan
Tel.: +81 3 3964 3241 (ext. 3503)
Fax: +81 3 3964 2188
e-mail: ishii@pet.tmig.or.jp

Accepted for publication April 9, 2008

Introduction

Essential blepharospasm (EB) is a form of focal dystonia characterized by involuntary spasms of orbicularis oculi muscles. Many studies suggested that dysfunction of dopamine D_2 receptor-mediated inhibition of pathways involving the putamen, which in turn most probably activates the basal ganglia-cortical motor circuit (Fig. 1A) (1), might cause dystonia (2, 3). Decreased dopamine D_2 receptor binding has been reported in patients with primary focal dystonias other than EB (4, 5).

The purpose of this study was to investigate whether dopamine D_2 receptor binding was altered in EB as in the other forms of dystonia. Therefore, we studied the binding of [^{11}C]raclopride (RAC), a dopamine D_2 receptor radioligand, in EB patients by using positron emission tomography (PET). We specifically focused on the regional difference in dopamine D_2 receptor binding within the striatum because it has not been examined in the previous studies on the other forms of dystonia (4, 5). Additionally, the striatum has a somatotopic organization (6), and each type of focal dystonia has typically localized symptoms; thus, we hypothesized that the specific site of striatal dysfunction would correspond to the part of the body that developed dystonia.

Materials and methods

Subjects

We studied eight patients with bilateral EB [two men and six women, mean age ± standard deviation (SD) = 54.1 ± 4.3 years] and eight age-matched healthy volunteers (two men and six women, mean age ± SD = 52.4 ± 4.0 years) as controls. None of the subjects had any additional neurologic disorder and any family history of dystonic disorders. None of them were taking or had taken any medications known to affect dopamine receptor binding or that could induce dystonia in these subjects (7). All but two patients

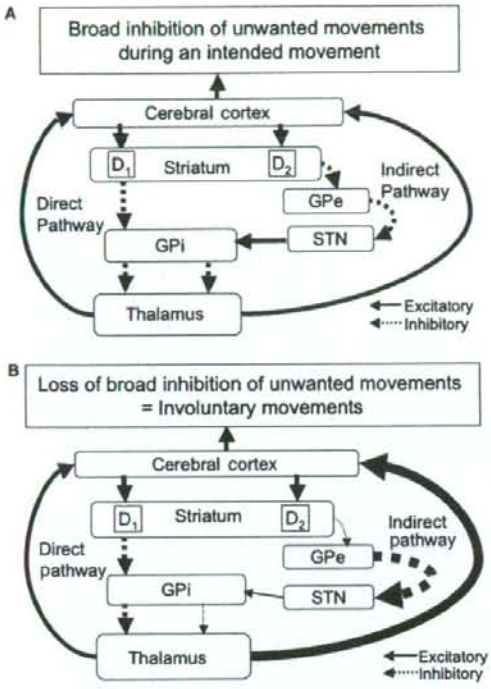

Figure 1. The role of the dopamine D_2 receptor-mediated indirect pathway on the activity of the basal ganglia-cortical motor circuit [adapted from Todd and Perlmutter (2) and Perlmutter and Mink (3)]. (A) The proposed circuit model under normal conditions. (B) Predicted changes in activity following decreased D_2 receptor binding under essential blepharospasm conditions. Solid and dashed lines indicate excitatory and inhibitory connections, respectively. The width of the lines depicts the amount of neuronal activity. D_1, dopamine D_1 receptor; D_2, dopamine D_2 receptor; GPe, external globus pallidus; GPi, internal globus pallidus; STN, subthalamic nucleus.

had been treated previously with local injections of botulinum toxin type A in the affected muscles, and the last botulinum toxin type A injection had been taken at least 1 month before the study. At the time of the PET study, we evaluated the severity and frequency of EB according to the classification of Jankovic et al. (8) and observed that all the patients demonstrated symmetric symptoms in terms of the Jankovic scores. The clinical details of the patients are summarized in Table 1. This study protocol was approved by the Institutional Ethics Committee. All the procedures conformed to the tenets of the Declaration of Helsinki. Informed consent was obtained from each subject prior to participation in the PET study.

Magnetic resonance imaging (MRI) was performed just prior to the PET measurement by using a 1.5 T scanner Signa Excite (General Electric, Milwaukee, WI, USA) to rule out organic brain disorders and for anatomic reference when setting regions of interest (ROIs) for PET data analysis. Transaxial images with T1-weighted contrast [three-dimensional spoiled gradient-recalled acquisition (3D-SPGR), repetition time (TR) = 9.2 ms, time to echo (TE) = 2.0 ms, matrix size = 256 × 256 × 124, voxel size = 0.94 × 0.94 × 1.3 mm] and T2-weighted contrast (TR = 3000 ms, TE = 100 ms, matrix size = 256 × 256 × 20, voxel size = 0.7 × 0.7 × 6.5 mm) were obtained. None of the subjects demonstrated any abnormalities with regard to brain morphology and intensities.

PET data acquisition

The PET scans were obtained using the Headtome-V SET 2400W scanner (Shimadzu, Kyoto, Japan) at the Positron Medical Center, Tokyo Metropolitan Institute of Gerontology. Each subject was placed in the supine position with their eyes closed in the PET camera gantry and their heads immobilized with a customized head holder for aligning the orbitomeatal line parallel to the scanning plane.

Table 1 Patient characteristics

Case no.	Age (years)	Gender	Duration of disease (years)	Last treatment with botulinum toxin	Strength of the eyelid spasm	
					Severity (right/left)	Frequency (right/left)
1	47	F	4	3 months	1/1	1/1
2	49	F	4	No treatment	3/3	3/3
3	54	M	3	3 months	1/1	1/1
4	54	F	4	2 months	2/2	1/1
5	55	F	10	No treatment	3/3	3/3
6	56	M	10	3 months	3/3	3/3
7	58	F	6	1 month	1/1	1/1
8	60	F	4	2 months	2/2	1/1

Severity and frequency of the spasm was rated on a 0 (=none) to 4 (=severe) scale. M, male; F, female.

The scanner room was dimly illuminated and quiet throughout the testing. After attenuation was corrected using a transmission scan with a $^{68}Ga/^{68}Ge$ rotating source, a bolus of 327 ± 74 MBq RAC was injected intravenously into the subjects. The preparation method of RAC is described elsewhere (9). The specific activity and amount of the injected cold material were 67.2 ± 73.2 MBq/nmol and 10.5 ± 9.9 nmol, respectively. A 15-min emission scan in three-dimensional acquisition mode was initiated 40 min after injecting the tracer when specific binding of the tracer reached pseudoequilibrium. We obtained 50 transaxial images with an interslice interval of 3.125 mm (10). The reconstructed image resolution was 4.5 × 4.5 × 6.5 mm at full-width half-maximum.

Data processing and statistical analysis

The PET images were registered three-dimensionally to the individual 3D-SPGR MRI images with the Automatic Multimodality Image Registration program (11). The 3D-SPGR MRI images were resliced at the same position as the registered individual PET images for anatomic reference.

The ROIs were defined interactively on the PET slices by visual inspection with reference to a standard neuroanatomical atlas and the reconstructed MRI images. As shown in Fig. 2, the ROIs were bilaterally located over the caudate (one 8-mm-diameter circular region), anterior putamen (two 6-mm-diameter circular regions), and posterior putamen (two 6-mm-diameter circular regions) on each slice of the three contiguous slices that revealed the maximum RAC uptake densities. Cerebellar ROIs (four 10-mm-diameter circular regions over the cerebellar lobe of each hemisphere) were also defined on each slice of the three contiguous slices. As the density of the dopamine D_2 receptors in the cerebellum is negligible, the cerebellum was used as a reference area. For each ROI of the striatum, the RAC uptake index was calculated using the following formula:

$$\text{RAC uptake index} = (\text{target ROI activity} - \text{cerebellar ROI activity}) / \text{cerebellar ROI activity}$$

It has been demonstrated that the RAC uptake index is linearly correlated with the binding potential estimated by a compartment model and dynamic scanning data (12, 13). The RAC uptake indices of left and right ROIs were averaged because they were not significantly different between the two

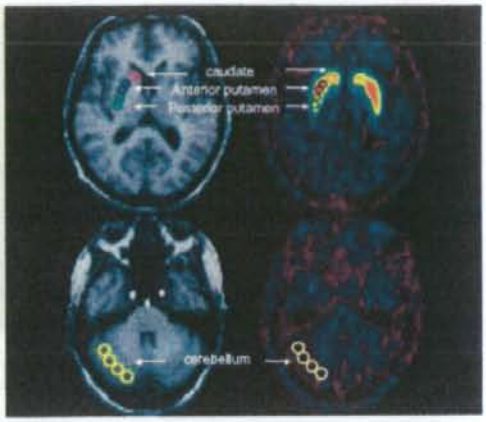

Figure 2. Regions of interest (ROIs) placed on the magnetic resonance and [^{11}C]raclopride positron emission tomography images. The structures on which the ROIs were bilaterally located included the caudate, anterior putamen, posterior putamen, and cerebellum in three contiguous slices. One side of the ROIs has been displayed for demonstration.

hemispheres in both the EB and control groups (paired t-test, $P > 0.1$), and the severity and frequency of EB were symmetric between left and right eyelid spasm in all the patients.

Statistical significance between the EB patients and controls was determined using the Mann–Whitney U-test with Bonferroni multiple-comparison correction. Values of $P < 0.017 = 0.05/3$ were considered statistically significant.

Results

Typical images and the results of the ROI analysis based on the PET images are shown in Figs 3 and 4, respectively. The mean RAC uptake indices ± SD in the EB and control groups were 2.59 ± 0.28 and 2.93 ± 0.24 for the caudate, 3.26 ± 0.17 and 3.68 ± 0.29 for the anterior putamen, and 3.22 ± 0.21 and 3.60 ± 0.29 for the posterior putamen, respectively. The uptake indices in the EB group were significantly reduced by 11.7% in the caudate ($P < 0.005$), 11.6% in the anterior putamen ($P < 0.0001$), and 10.3% in the posterior putamen ($P < 0.005$) relative to indices of the control group. There was no correlation between the severity and duration of EB and the degree of the RAC uptake index in different parts of the striatum.

Discussion

We observed significant decreased RAC uptake indices of the caudate and putamen in the EB patients when compared with the normal controls.

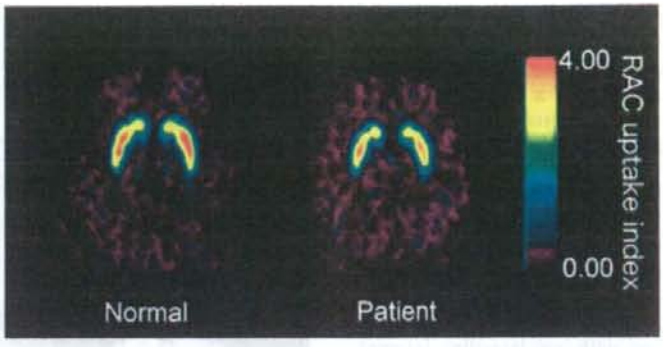

Figure 3. Representative [^{11}C]raclopride (RAC) uptake index images in a normal subject (left) and in a patient (case 1) with essential blepharospasm (right). RAC uptake indices are reduced in the caudate, anterior putamen, and posterior putamen of the patient.

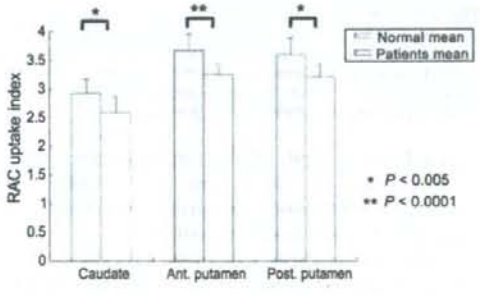

Figure 4. Mean [^{11}C]raclopride (RAC) uptake indices ± SD. The RAC uptake index is decreased by approximately 10% in each region of the striatum in patients with essential blepharospasm.

The number of subjects in the present study is fewer than in earlier studies. We consider our results to be sufficiently reliable because we strictly selected patients with bilateral and symmetric EB without confounding other types of dystonia or other neurologic disorders. Some patients in this study were treated with botulinum toxin. Botulinum toxin acts on the peripheral neuromuscular junction by a presynaptic blockage and botulinum toxin does not cross the blood–brain barrier. Previous studies have reported no significant alterations in the level of regional cerebral blood flow after botulinum toxin treatment in patients with dystonia (14, 15). There was no significant difference in the mean RAC uptake index between the treated and the untreated patients in our study. Therefore, we suppose that the previous treatment with botulinum toxin has minimum direct influence on the RAC uptake in this study. However, further study is required to clarify its indirect functional effect on the basal ganglia-cortical motor circuit. Decreased RAC uptake indices may be interpreted as decreased D_2 receptor density and/or as lowered D_2 receptor affinity for RAC. In addition, decreased RAC uptake indices may be ascribable to increased endogenous dopamine release, because endogenous dopamine competes for RAC-binding sites (16). An additional theoretical possibility is an increased partition volume of RAC in the reference region. Although we have to consider the possibility of all these factors that can modify RAC uptake in EB to varying degrees, previous studies have supported the former two possibilities that a hypofunction of D_2-mediated dopaminergic pathways contributes to the pathophysiology of dystonia (2, 3). Several genetic mutations of dystonia produce dopamine deficiency without nigrostriatal neuron loss (17, 18). Dopa-responsive dystonia has remarkable symptomatic response to levodopa with well-preserved nigrostriatal neurons (19). However, it is unlikely that decreased dopamine activity or D_2 receptor binding solely would cause EB, because the following inconsistent results have been reported. Dopamine levels markedly decrease in Parkinson's disease, but EB does not predispose to developing Parkinson's disease (20). RAC-PET studies in dopa-responsive dystonia have shown increased RAC uptake (21, 22). In an RAC-PET study in non-manifesting carriers of the DYT1 dystonia gene mutation, dopamine D_2 receptor binding was reduced (23), and only approximately 30% of DYT1 carriers developed clinical manifestations. These observations suggest that functional imbalance in dopaminergic pathways might be more important in causing dystonia than simple alteration in dopamine release or in D_2 receptor binding.

The basal ganglia-cortical motor circuit model (Fig. 1A) (1) might explain the role of imbalance of dopaminergic pathways in EB. This motor circuit

operates during normal voluntary movements and maintains posture by controlling muscle tonus adequately. The circuit comprises two major parallel pathways, i.e., direct and indirect pathways that connect the striatum to the internal globus pallidus (GPi). The dopamine input to the striatum differentially modifies the activity of both these pathways. When a voluntary movement is initiated, the indirect pathway mediated by the dopamine D_2 receptors stimulates the GPi, resulting in broad inhibition of unwanted competing movements during an intended movement. In contrast, the direct pathway mediated by dopamine D_1 receptors inhibits the GPi, resulting in the focused facilitation of a selected voluntary movement (3, 24). An adequate balance between the activities of both these pathways is essential for normal motor control. Imbalance between D_1 and D_2-mediated effects might activate the thalamic excitation of the cortex and probably lead to a reduction in inhibiting unwanted movements during an intended movement (25). This alteration might cause the involuntary movements observed in EB (Fig. 1B) (2, 3).

We defined ROIs on three subregions of the striatum for precise localization of the regions within the striatum that are responsible for EB. We hypothesized that the specific site of striatal dysfunction would correspond to the part of the body that developed dystonia because the striatum has somatotopic organization (6) and because each type of focal dystonia has typically localized symptoms. EB is characterized by involuntary spasms of the orbicularis oculi muscles. Patients with writer's cramp experience excessive cocontractions of the agonist and antagonist hand muscles during writing. Spasmodic torticollis is the involuntary rotation of the head into abnormal postures. Despite these facts, our results revealed no significant inter-regional variations in RAC binding among the subregions of the striatum. There must be additional factors that cause localized expression in each type of dystonia.

Recently, several lines of evidence have indicated that other neurotransmitter pathways contributed to the pathophysiology of dystonia. Polymorphism of the dopamine D_5 receptor gene might be associated with focal dystonia (26). Gamma-aminobutyric acid (GABA) levels in the sensorimotor cortex and striatum were decreased in patients with focal dystonia (27). An injection of bicuculline, a $GABA_A$ receptor antagonist, into the monkey thalamus induced dystonic symptoms contralaterally (28). On the other hand, Zolpidem, which is an imidazopyridine with a short hypnotic action used for treating insomnia, binds to $GABA_A$ receptors and might improve EB (29). However, none of these can independently explain the pathophysiology of dystonia. Dysfunction of dopaminergic or other neurotransmitter pathways might be necessary but not sufficient to lead to the clinical presentation in dystonia. Dystonia might develop by the combination of a predisposing factor and a second precipitating event. An animal model explains that a combination of both dysfunction of dopamine activity and orbicularis oculi weakening causes EB (30). In humans, dopamine D_2 receptor dysfunction could constitute a permissive condition, and an external ophthalmic insult, such as dry eye or slight weakening of the orbicularis oculi muscle, could constitute the subsequent precipitating condition. Even if neither of these modifications can independently cause spasms of the eyelid, when they occur in combination, they might be able to induce forceful blinking and spasms of the eyelid in EB. It would be helpful to understand the pathophysiological mechanisms of EB with this multifactorial model in order to develop effective therapeutic strategies.

Based on our finding of a significant decrease in dopamine D_2 receptor binding by ~10%, we hypothesize that this finding might be one of the important predisposing factors for EB and that other factors might be involved in EB development. In conclusion, signal processing through the indirect pathway of the motor circuit can be influenced at many different points, and decreased dopamine D_2 receptor binding might play an important role in the pathophysiology of EB.

Acknowledgements

We thank Yuichi Kimura, Keiichi Kawasaki, Yoko Saito, and Hiroko Tsukinari for their technical assistance and useful discussions.

References

1. Alexander GE, Crutcher MD. Functional architecture of basal ganglia circuits: neural substrates of parallel processing. Trends Neurosci 1990;13:266–71.
2. Todd RD, Perlmutter JS. Mutational and biochemical analysis of dopamine in dystonia: evidence for decreased dopamine D_2 receptor inhibition. Mol Neurobiol 1998; 16:135–47.
3. Perlmutter JS, Mink JW. Dysfunction of dopaminergic pathways in dystonia. Adv Neurol 2004;94:163–70.
4. Perlmutter JS, Stambuk MK, Markham J et al. Decreased [^{18}F]spiperone binding in putamen in idiopathic focal dystonia. J Neurosci 1997;17:843–50.
5. Naumann M, Priker W, Reiners K, Lange KW, Becker G, Brucke T. Imaging the pre- and postsynaptic side of striatal dopaminergic synapses in idiopathic cervical dystonia: a SPECT study using [^{123}I]epidepride and [^{123}I]beta-CIT. Mov Disord 1998;13:319–23.

6. Maillard L, Ishii K, Bushara K, Waldvogel D, Schulman AE, Hallett M. Mapping the basal ganglia: fMRI evidence for somatotopic representation of face, hand, and foot. Neurology 2000;**55**:377–83.
7. Casey DE. Pathophysiology of antipsychotic drug-induced movement disorders. J Clin Psychiatry 2004;**64**(Suppl.9):25–8.
8. Jankovic J, Havins WE, Wilkins RB. Blinking and blepharospasm. Mechanism, diagnosis, and management. JAMA 1982;**248**:3160–4.
9. Langer O, Någren K, Dolle F et al. Precursor synthesis and radiolabelling of the dopamine D_2 receptor ligand [^{11}C]raclopride from [^{11}C]methyl triflate. J Labelled Comp Radiopharm 1999;**42**:1183–93.
10. Fujiwara T, Watanuki S, Yamamoto S et al. Performance evaluation of a large axial field-of-view PET scanner: SET-2400W. Ann Nucl Med 1997;**11**:307–13.
11. Ardekani BA, Braun M, Hutton BF, Kanno I, Iida H. A fully automatic multimodality image registration algorithm. J Comput Assist Tomogr 1995;**19**:615–23.
12. Farde L, Eriksson L, Blomquist G, Halldin C. Kinetic analysis of central [^{11}C] raclopride binding to D_2-dopamine receptors studied by PET: a comparison to the equilibrium analysis. J Cereb Blood Flow Metab 1989; **9**:696–708.
13. Brooks DJ, Ibanez V, Sawle GV et al. Striatal D_2 receptor status in patients with Parkinson's disease, striatonigral degeneration, and progressive supranuclear palsy, measured with ^{11}C-raclopride and positron emission tomography. Ann Neurol 1992;**31**:184–92.
14. Ceballos-Baumann AO, Sheean G, Passingham RE et al. Botulinum toxin does not reverse the cortical dysfunction associated with writer's cramp. A PET study. Brain 1997;**120**:571–80.
15. Ridding MC, Sheean G, Rothwell JC. Changes in the balance between motor cortical excitation and inhibition in focal, task specific dystonia. J Neurol Neurosurg Psychiatry 1995;**59**:493–8.
16. Seeman P, Guan HC, Niznik HB. Endogenous dopamine lower the dopamine D2 receptor density as measured by [3H]raclopride: implications for positron emission tomography of the human brain. Synapse 1989;**3**:96–7.
17. Nygaard TG. Dopa-responsive dystonia. Curr Opin Neurol 1995;**8**:310–3.
18. Knappskog PM, Flatmark T, Mallet J, Lüdecke B, Bartholome K. Recessively inherited L-DOPA-responsive dystonia caused by a point mutation (Q381K) in the tyrosine hydroxylase gene. Hum Mol Genet 1995;**4**:1209–12.
19. Rajput AH, Gibb WR, Zhong XH et al. Dopa-responsive dystonia: pathological and biochemical observations in a case. Ann Neurol 1994;**35**:396–402.
20. Soonawala N, Bhatia KP, Yeung JH, Quinn NP, Marsden CD. Idiopathic blepharospasm does not lead to a parkinsonian syndrome: results of a questionnaire-based follow-up study. J Neurol 1999;**246**:283–6.
21. Kishore A, Nygaard TG, de la Fuente-Fernandez R et al. Striatal D2 receptors in symptomatic and asymptomatic carriers of dopa-responsive dystonia measured with [11C]-raclopride and positron emission tomography. Neurology 1998;**50**:1028–32.
22. Rinne JO, Ilvanainen M, Metsähonkala L et al. Striatal dopaminergic system in dopa-responsive dystonia: a multitracer PET study shows increased D2 receptors. J Neural Transm 2004;**111**:59–67.
23. Asanuma K, Ma Y, Okulski J et al. Decreased striatal D_2 receptor binding in non-manifesting carriers of the DYT1 dystonia mutation. Neurology 2005;**64**:347–9.
24. Mink JW. The basal ganglia: focused selection and inhibition of competing motor programs. Prog Neurobiol 1996;**50**:381–425.
25. Geday J, Ostergaard K, Johnsen E, Gjedde A. STN-stimulation in Parkinson's disease restores striatal inhibition of thalamocortical projection. Hum Brain Mapp (in press).
26. Misbahuddin A, Placzek MR, Chaudhuri KR, Wood NW, Bhatia KP, Warner TT. A polymorphism in the dopamine receptor DRD5 is associated with blepharospasm. Neurology 2002;**58**:124–6.
27. Levy LM, Hallett M. Impaired brain GABA in focal dystonia. Ann Neurol 2002;**51**:93–101.
28. Macia F, Escola L, Guehl D, Michelet T, Bioulac B, Burbaud P. Neuronal activity in the monkey motor thalamus during bicuculline-induced dystonia. Eur J Neurosci 2002;**15**:1353–62.
29. Garretto NS, Bueri JA, Rey RD, Arakaki T, Nano GV, Mancuso M. Improvement of blepharospasm with Zolpidem. Mov Disord 2004;**19**:967–8.
30. Schicatano EJ, Basso MA, Evinger C. Animal model explains the origins of the cranial dystonia benign essential blepharospasm. J Neurophysiol 1997;**77**:2842–6.

Ann Nucl Med (2008) 22:191–200
DOI 10.1007/s12149-007-0099-7

ORIGINAL ARTICLE

Influence of mild hyperglycemia on cerebral FDG distribution patterns calculated by statistical parametric mapping

Keiichi Kawasaki · Kenji Ishii · Yoko Saito
Keiichi Oda · Yuichi Kimura · Kiichi Ishiwata

Received: 2 October 2007 / Accepted: 29 November 2007
© The Japanese Society of Nuclear Medicine 2008

Abstract
Objective In clinical cerebral 2-[^{18}F]fluoro-2-deoxy-D-glucose positron emission tomography (FDG-PET) studies, we sometimes encounter hyperglycemic patients with diabetes mellitus or patients who have not adhered to the fasting requirement. The objective of this study was to investigate the influence of mild hyperglycemia (plasma glucose range 110–160 mg/dl) on the cerebral FDG distribution patterns calculated by statistical parametric mapping (SPM).
Methods We studied 19 healthy subjects (mean age 66.2 years). First, all the subjects underwent FDG-PET scans in the fasting condition. Then, 9 of the 19 subjects (mean age 64.3 years) underwent the second FDG-PET scans in the mild hyperglycemic condition. The alterations in the FDG-PET scans were investigated using SPM- and region of interest (ROI)-based analyses. We used three reference regions: (1) SPM global brain (SPMgb) used for SPM global mean calculation, (2) the gray and white matter region computed from magnetic resonance image (MRIgw), and (3) the cerebellar cortex (Cbll).
Results The FDG uptake calculated as the standardized uptake value (average) in SPMgb, MRIgw, and Cbll regions in the mild hyperglycemic condition was 42.7%, 41.3%, and 40.0%, respectively, of that observed in the fasting condition. In SPM analysis, the mild hyperglycemia was found to affect the cerebral distribution patterns of FDG. The FDG uptake was relatively decreased in the gray matter, mainly in the frontal, temporal, and parietal association cortices, posterior cingulate, and precuneus in both SPMgb- and MRIgw-reference-based analyses. When Cbll was adopted as the reference region, those decrease patterns disappeared. The FDG uptake was relatively increased in the white matter, mainly in the centrum semiovale in all the reference-based analyses.
Conclusions It is noteworthy that the FDG distribution patterns were altered under mild hyperglycemia in SPM analysis. The decreased uptake patterns in SPMgb- (SPM default) and MRIgw-reference-based analyses resembled those observed in Alzheimer's disease. Under mild hyperglycemia, we can recommend Cbll as the reference region to detect decreased uptake patterns. We should pay special attention to controlling the diet condition, monitoring hyperglycemia, and optimizing the reference region in SPM analysis, particularly in the diagnosis of early Alzheimer's disease in clinical FDG-PET.

Keywords FDG-PET · Mild hyperglycemia · Distribution pattern · Statistical parametric mapping · Alzheimer's disease

K. Kawasaki (✉) · K. Ishii · Y. Saito · K. Oda · Y. Kimura · K. Ishiwata
Positron Medical Center, Tokyo Metropolitan Institute of Gerontology, 1-1 Naka-cho, Itabashi-ku, Tokyo 173-0022, Japan
e-mail: kawasaki@pet.tmig.or.jp

Introduction

Cerebral 2-[^{18}F]fluoro-2-deoxy-D-glucose positron emission tomography (FDG-PET) examinations are widely used for the diagnosis of neurological disorders such as dementia, epilepsy, and tumors. A high plasma glucose level and diet-enhanced FDG uptake by extra-brain tissues decrease the FDG uptake in the brain and reduce the quality of brain images [1, 2]. So the examinations

are usually carried out after a 4–6-h fast to give a low plasma glucose concentration. However, FDG-PET is sometimes carried out in hyperglycemic patients with diabetes mellitus, or in patients who have not adhered to the fasting requirement. Nevertheless, in most cases, the glucose level is still less than the criterion of hyperglycemia (plasma glucose > 160 mg/dl) as described in the "European Association of Nuclear Medicine Procedure Guidelines for Brain Imaging using [^{18}F]FDG" [2]. In such mild hyperglycemic cases, it is usually assumed that the FDG distribution pattern in the brain in the fasting condition is maintained regardless of plasma glucose levels.

In recent years, clinical examinations require the detection of subtle abnormalities of regional cerebral FDG uptake in patients with neurological disorders such as early Alzheimer's disease and refractory focal epilepsy. Usually, static (semi-quantitative) images of FDG are used, and when data from age-matched normal controls are available, the data from each patient are evaluated by statistical approaches such as statistical parametric mapping (SPM) [3] and three-dimensional (3D) stereotactic surface projection (3D-SSP) techniques [4].

In the course of the SPM analysis in the FDG-PET studies, we have encountered patients who had not fasted but whose plasma glucose level was no more than 160 mg/dl. However, the results of the SPM analysis sometimes showed abnormalities different from the clinical presentation.

With regard to the relationship between cerebral glucose metabolism and the plasma glucose level, Hasselbalch et al. [6] measured the global cerebral metabolic rate of glucose (CMRglc) and regional CMRglc (rCMRglc) on the basis of the Sokoloff model [5] in normoglycemic control condition (plasma glucose 97 mg/dl) and in an acute hyperglycemic condition (270 mg/dl) in six normal subjects. They reported that during acute hyperglycemia, when compared with the normoglycemia, with the exception of a significant increase (42%) in the white matter in the centrum semiovale, the global CMRglc and rCMRglc in the cortical and subcortical gray matter regions did not change. However, if a significant increase occurs unexpectedly in the white matter in the centrum semiovale during hyperglycemia, as demonstrated by Hasselbalch et al. [6], the subjects whose plasma glucose level is not controlled to the fasting level may be erroneously diagnosed by the statistical approaches. Therefore, it is necessary to investigate whether the plasma glucose levels alter the regional cerebral FDG uptake, thereby possibly influencing the FDG distribution patterns obtained by using the statistical approaches.

In the present study, we focused on the glucose levels less than the aforementioned criterion of hyperglycemia (>160 mg/dl) [2]. As a fasting glucose level from 70 mg/dl to 109 mg/dl in plasma is generally considered to be normal, we defined the plasma glucose level from 110 mg/dl to 160 mg/dl as mild hyperglycemia.

The objective of this study was to investigate the influence of plasma glucose levels within the mild hyperglycemia on the cerebral FDG distribution patterns, particularly the patterns obtained by using SPM analysis.

Materials and methods

Subjects and conditions

We studied 19 healthy subjects (6 men and 13 women) with a mean age of 66.2 years (range 48–80 years). All the subjects fulfilled the following criteria: (1) no history of diabetes mellitus, neurological or psychiatric disorders, head trauma, drug abuse, alcoholism, hypertension, or cardiac disease, (2) no medication, (3) found to be normal on physical and neurological examinations, (4) Mini-Mental State Examination score = 30, and (5) found to be normal on anatomical magnetic resonance imaging (MRI), i.e., 3D-MRI (described below) and T2-weighted MRI. This study was approved by the institutional Ethics Committee. A written informed consent was obtained from all the subjects before the study.

First all the subjects underwent FDG-PET scanning in the fasting condition (after >5-h fasting). Then, within 1 month, 9 of the 19 subjects (2 men and 7 women, mean age 64.3 years, range 48–80 years) underwent a second FDG-PET scanning in the mild hyperglycemic condition in which each subject first consumed a normal lunch 2–2.5 h prior to the FDG injection and was then orally administered 50 g glucose (TRELAN-G50, 150 ml; Ajinomoto Pharma, Tokyo, Japan) 30 min prior to the FDG injection. At PET measurement 1–2 ml of venous blood samples were drawn twice immediately prior to the intravenous FDG injection and 30 min following the injection (t = 0 min and 30 min, respectively), and the plasma glucose concentration was measured. The paired comparison between the fasting and mild hyperglycemic conditions was done using the data obtained from the 9 subjects scanned twice, and the comparisons between one scan in the fasting or hyperglycemic condition and the normal database were done between the data obtained from the 9 subjects and the data of the 19 subjects in the fasting condition.

Image acquisition

For all subjects, the 3D-MRI images with T1-weighted contrast were obtained with a 1.5-T Sigma Horizon scanner (GE, Milwaukee, WI, USA) using the following imaging parameters: matrix size 256 × 256 × 124 and voxel size 0.9375 × 0.9375 × 1.3 mm. The images were obtained using the 3D spoiled gradient echo protocol (TR/TE = 9.2 ms/2.0 ms) before the first FDG-PET scan.

FDG images were obtained with a PET scanner (SET 2400W; Shimadzu, Kyoto, Japan) in the 3D mode [image resolution: transverse full width at half-maximum (FWHM) = 4.4 mm, axial FWHM = 6.5 mm]. Forty-five minutes following the intravenous injection of FDG (130.4 ± 15.0 MBq), a 6-min emission scan was collected to create images with the following parameters: matrix size 128 × 128 × 50 and voxel size 2 × 2 × 3.125 mm. The attenuation was corrected by a transmission scan using a $^{68}Ga/^{68}Ge$ source. During the tracer-accumulation phase, the subjects remained supine, quiet, and motionless in a dimly lit and quiet (except for air-conditioner noise) room with their eyes open and ears unoccluded.

Image processing

Image processing and data analysis were performed using SPM2 (Functional Imaging Laboratory, London, UK) implemented on MATLAB (The MathWorks, Natick, MA, USA) and Dr. View (AJS, Tokyo, Japan). The tasks performed by SPM2 were MRI/PET coregistration, spatial normalization, spatial smoothing, MRI segmentation, normalization for reference region, and SPM analysis. The tasks performed by Dr. View were image masking and region of interest (ROI) analysis. All FDG images were spatially normalized and resampled (XYZ matrix 79 × 95 × 80 and voxel size 2 × 2 × 2 mm) using the FDG template which was created from the FDG images of 15 physically and psychiatrically healthy subjects (mean age 33.3 years, range 20–49 years) in accordance with a method described elsewhere [7]. Each 3D-MRI image was coregistered to the corresponding FDG image in the fasting condition and normalized to the FDG template using the parameters obtained from the spatial normalization of the corresponding FDG images.

To investigate alterations of regional FDG uptake and FDG distribution patterns, we used three kinds of image reference regions termed as SPMgb, MRIgw, and Cbll (Fig. 1). SPMgb (Fig. 1b) indicates the SPM global brain region used for the calculation of global mean in default in SPM program. SPMgb is defined implicitly in each image by using a two-step process: first the overall mean is computed, and then voxels measuring less than the quotient of the mean divided by 8 are deemed extracranial and are masked out. Thus, SPMgb is uniquely defined image-by-image. The global mean is then recomputed on the remaining voxels. MRIgw (Fig. 1c) indicates an MRI-based gray and white matter region computed using the segmentation function of SPM program and is defined for each subject separately. Cbll

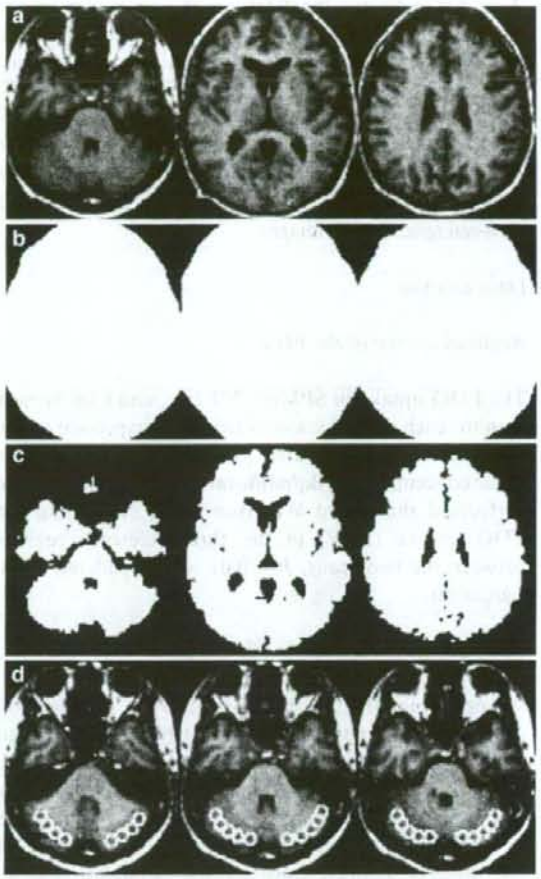

Fig. 1 An example of the brain regions investigated. **a** The space normalized 3D-magnetic resonance imaging (MRI) image of a subject. **b** Statistical parametric mapping global brain (SPMgb) computed from the 2-[^{18}F]fluoro-2-deoxy-D-glucose positron emission tomography (FDG-PET) image of the subject in the fasting condition in default in SPM program (smoothed using a Gaussian filter with a 16-mm full width at half-maximum). SPMgb in the mild hyperglycemic condition was nearly equal to that in the fasting condition (not shown). **c** MRIgw consisting of the gray and white matter regions computed from the 3D-MRI image of the subject using SPM segmentation function. **d** Cerebellar cortex [Cbll, region of interest (ROI) on cerebellar cortex] consisting of 48 circles 10 mm in diameter on five continuous slices

(Fig. 1d) indicates the ROI on the cerebellar cortex common to all spatially normalized images. It is noted that the MRIgw includes gray and white matter regions, whereas the SPMgb contains the entire intracranial contents including cerebrospinal fluid and orbit regions.

The subject mean of SPMgb, MRIgw, and Cbll of each FDG image after spatial normalization was normalized to be 50 to create SPMgb- MRIgw-, and Cbll-reference-based images.

Data analysis

Regional uptake of the FDG

The FDG uptake in SPMgb, MRIgw, and Cbll in each scan for each subject scanned twice was expressed as the standardized uptake value [SUV, body weight (g) × tissue concentration (Bq/ml)/total injected dose (Bq). We performed the paired Wilcoxon t test comparing the FDG uptake (SUV) in the three reference regions between the two scans; $P < 0.01$ was considered to be significant.

SPM-based analysis of the FDG uptake

We performed three global normalization processes on the basis of SPMgb-, MRIgw-, and Cbll-reference-based images. Those images were smoothed using a Gaussian filter with a 16-mm FWHM to increase the sensitivity and then we calculated the statistical parametric maps of the paired t test between the first and second scans of the subjects scanned twice by the "Population main effect: 2 cond's, 1 scan/cond" of SPM analysis design type ($P < 0.001$, uncorrected, extent threshold $k = 300$ voxels). We also calculated the statistical maps using "Compare-populations: 1 scan/subject (Ancova)" with age as a covariate between each scan in the fasting or mild hyperglycemic condition of the 9 subjects and the scans in the fasting condition of the other 18 of the 19 subjects (1 of the 19 subjects under comparison was excluded) using it as the normal database ($P < 0.01$, uncorrected, extent threshold $k = 300$ voxels).

ROI-based analysis of the FDG uptake

In the subjects scanned twice, the ROIs common to all normalized images were placed on the Cbll, centrum semiovale, and the frontal, temporal, and parietal cortices, and posterior cingulate/precuneus. The ROIs of the Cbll, centrum semiovale, and the frontal, temporal, and parietal cortices, and posterior cingulate/precuneus consisted of 48 circles 10 mm in diameter on 5 continuous slices, 26 on 5, 116 on 16, 116 on 17, 50 on 7, and 46 on 17, respectively. The relative FDG uptake in the ROIs was calculated in SPMgb-, MRIgw-, and Cbll-reference-based images without smoothing. For the ROI-based statistical analysis, the paired Wilcoxon t test was performed for each of the six ROIs between two scans; $P < 0.05$ with Bonferroni correction (total number of comparisons = 6, new alpha level = 0.0083) was considered to be significant.

Results

Fasting and mild hyperglycemic conditions

The plasma glucose concentration was significantly increased in the mild hyperglycemic condition: fasting scan (19 subjects), 91.7 ± 4.6 mg/dl at $t = 0$ min and 90.8 ± 5.5 mg/dl at $t = 30$ min; fasting scan (9 subjects scanned twice within 19 subjects), 90.0 ± 4.4 mg/dl at $t = 0$ min and 90.9 ± 6.9 mg/dl at $t = 30$ min; and mild hyperglycemic scan (9 subjects), 136.1 ± 10.5 mg/dl at $t = 0$ min, 138.1 ± 14.0 mg/dl at $t = 30$ min.

Three image reference regions and the FDG uptake

Figure 1 represents the space normalized 3D-MRI image of a subject and the three defined image reference regions (SPMgb, MRIgw, and Cbll). The SPMgb regions in both the fasting and mild hyperglycemic conditions were nearly equal.

The FDG uptake (SUV) in the three reference regions decreased greatly in the mild hyperglycemic condition ($P < 0.01$, Fig. 2). The SUV values in the SPMgb, MRIgw, and Cbll in the mild hyperglycemic condition were 42.7%, 41.3%, and 40.0%, respectively, of those observed in the fasting condition.

Paired comparison between the fasting and mild hyperglycemic conditions

First, the paired t test between the fasting and mild hyperglycemic conditions was performed by SPM, and the results are shown in Fig. 3 ($P < 0.001$, uncorrected, $k = 300$). In the contrast "uptake in the mild hyperglycemic condition < uptake in the fasting condition (uptake in M.hygl < uptake in Fasting)", the uptake in the gray matter and cerebellar cortex regions greatly decreased in SPMgb-reference-based analysis (Fig. 3a), and clear decreases were detected in the frontal, temporal, and parietal cortices, posterior cingulate, and precuneus in MRIgw-reference-based analysis (Fig. 3b). However, no decreased uptake pattern was detected in Cbll-reference-based analysis (not shown). In the contrast "uptake in

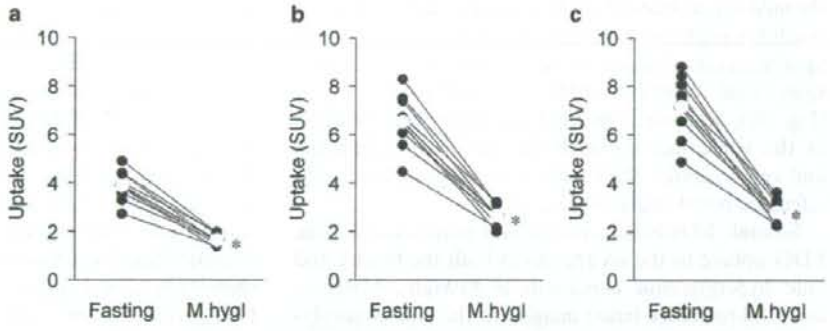

Fig. 2 FDG uptake (standardized uptake value) in SPMgb (**a**), MRIgw (**b**), and Cbll (**c**), respectively. The uptake was compared in the nine subjects scanned twice in the fasting and mild hyperglycemic (M.hygl) conditions. *Solid circles* represent individual subjects, and *open circles* represent the average ($n = 9$). $^*P < 0.01$ (paired Wilcoxon t test)

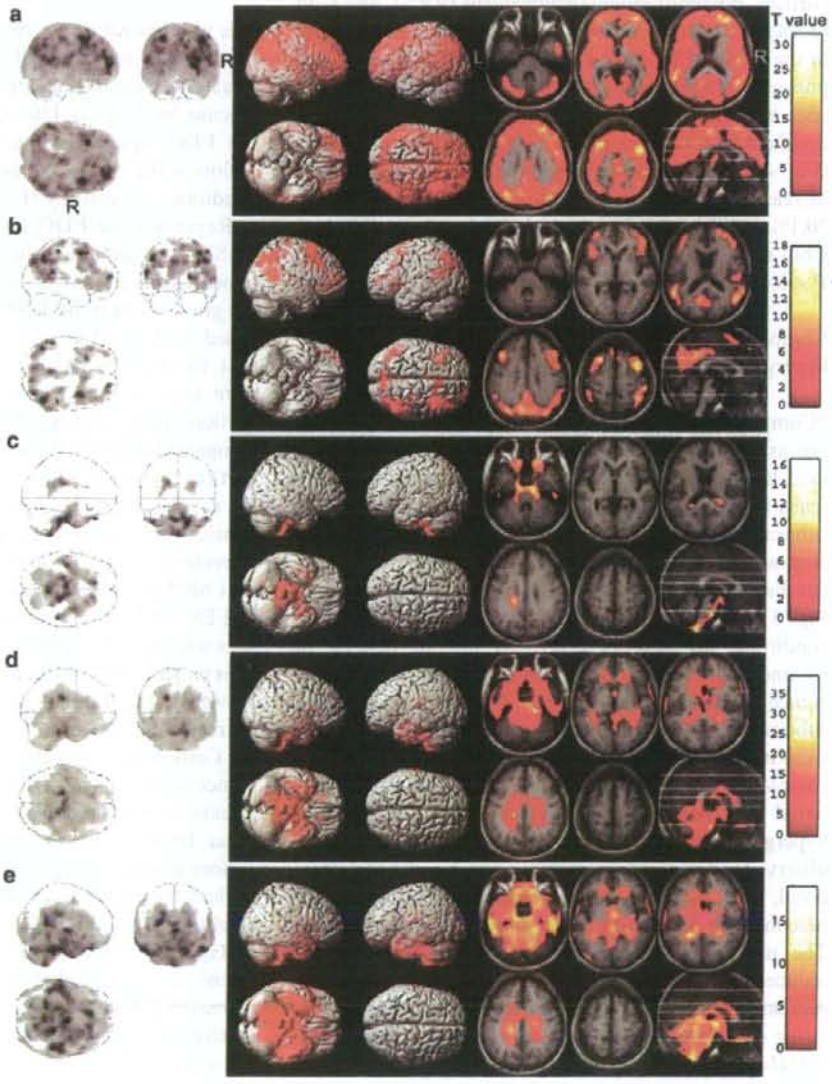

Fig. 3 SPM paired t tests "uptake in M.hygl < uptake in Fasting" in SPMgb- (**a**) and MRIgw- (**b**) reference-based analyses, and "uptake in M. hygl > uptake in Fasting" in SPMgb- (**c**), MRIgw- (**d**), and Cbll- (**e**) reference-based analyses. No decreased uptake pattern was detected in the mild hyperglycemic condition in Cbll-reference-based analysis (not shown). The SPM paired t tests were performed in the nine subjects scanned twice in the fasting and mild hyperglycemic conditions ($P < 0.001$, uncorrected; $k = 300$)

the mild hyperglycemic condition > uptake in the Fasting condition (uptake in M.hygl > uptake in Fasting)", the uptake increased in the centrum semiovale and cerebrospinal fluid regions in SPMgb-reference-based analysis (Fig. 3c), whereas significant increases were revealed in the white matter, cerebellar medullary substance, and cerebrospinal fluid regions in MRIgw- and Cbll-reference-based analyses (Fig. 3d, e).

Second, ROI-based analysis was performed for the FDG uptake in the six regions in both the fasting and mild hyperglycemic conditions in SPMgb-, MRIgw-, and Cbll-reference-based images. In the mild hyperglycemic condition, the uptake significantly decreased in the frontal (9.9%), temporal (7.6%), and parietal (9.2%) cortices, posterior cingulate/precuneus (9.9%), and Cbll (7.8%) in SPMgb-reference-based images (Fig. 4a), and in the frontal (5.6%) and temporal (3.2%) cortices, and posterior cingulate/precuneus (5.4%) in MRIgw-reference-based images (all $P < 0.05$, Fig. 4b), but no decreased uptake ROI was revealed in Cbll-reference-based images (Fig. 4c). On the other hand, the uptake significantly increased in the centrum semiovale: 10.8%, 16.1%, and 20.1% in SPMgb- (Fig. 4a), MRIgw- (Fig. 4b), and Cbll- (Fig. 4c) reference-based images, respectively (all $P < 0.05$).

Comparison between one scan in the fasting or mild hyperglycemic condition and the normal database

"Compare-populations: 1 scan/subject (Ancova)" with age as a covariate between each scan in the fasting or mild hyperglycemic condition of the 9 subjects and the scans in the fasting condition of the other 18 of the 19 subjects was performed by SPM, and the results in the contrast "uptake of one scan < uptake of the normal database" are shown on the sagittal projection in Fig. 5 ($P < 0.01$, uncorrected, $k = 300$). In the fasting condition, no notably decreased uptake pattern in common with nine subjects was detected in SPMgb-reference-based analysis (Fig. 5a). The spots observed in subjects 1, 4, 6, 7, and 9 were considered to be derived from individual morphological deviations that were not completely fitted to the FDG-PET template when compared with MRI images of each subject. In the mild hyperglycemic condition, significant decreases were observed in the association cortices such as frontal, temporal, and parietal cortices, posterior cingulate, and precuneus in SPMgb-reference-based analysis (Fig. 5b). The regions showing decreased uptake were greatly reduced in MRIgw-reference-based analysis, but the decreases were observed in the association cortices, posterior cingulate, and precuneus in some subjects (Fig. 5c). However, no decreased uptake patterns in any subjects were revealed in Cbll-reference-based analysis (not shown).

The results in the contrast "uptake of one scan > uptake of the normal database" were as follows (figures not shown). In the fasting condition, no notably increased uptake in common with nine subjects was detected. In the mild hyperglycemic condition, slight increases were observed in the white matter, cerebellar medullary substance, and cerebrospinal fluid regions in SPMgb-reference-based analysis in some subjects. The regions showing increased uptake spread widely in MRIgw- and Cbll-reference-based analyses.

Discussion

It is well known that a high plasma glucose concentration globally reduces FDG uptake in the brain [1, 2]. In this study, we confirmed that mild hyperglycemia (plasma glucose levels from 110 mg/dl to 160 mg/dl) decreased the FDG uptake in the SPMgb, MRIgw, and Cbll regions to 42.7%, 41.3%, and 40.0% of that in the fasting condition, respectively (Fig. 2).

Regarding the FDG distribution patterns calculated by SPM, we obtained the following findings. The mild hyperglycemia relatively decreased the FDG uptake in the gray matter in both SPMgb- and MRIgw-reference-based analyses (Figs. 3a, b, 4b, c). It should be noted that the regions showing relatively decreased uptake were the frontal, temporal, and parietal association cortices, posterior cingulate, and precuneus. It is well recognized that rCMRglc decreases in these association cortices are observed in Alzheimer's disease [8–12], and the decrease in the posterior cingulate and precuneus is considered to be an early sign of this disorder [13, 14]. Therefore, these findings demonstrate the possibility that SPMgb- or MRIgw-reference-based SPM analysis in FDG-PET could erroneously diagnose normal subjects whose plasma glucose levels were not below 110 mg/dl as patients with the early stages of Alzheimer's disease. However, the mild hyperglycemia did not reveal any decreases of FDG uptake in Cbll-reference-based analysis. Considering this result, we can recommend Cbll-reference-based analysis in the diagnosis of early Alzheimer's disease in the mild hyperglycemic condition. On the other hand, when we calculated the uptake increase regions in the mild hyperglycemic condition, the increases in the white matter, cerebellar medullary substance, and cerebrospinal fluid regions were detected, strongly, in MRIgw- and Cbll-reference-based analyses (Fig. 3c–e). Then, we realized that it would be difficult to detect increased uptake patterns characteristic of some degenerative diseases in SPM analysis in the mild hyperglycemic condition.

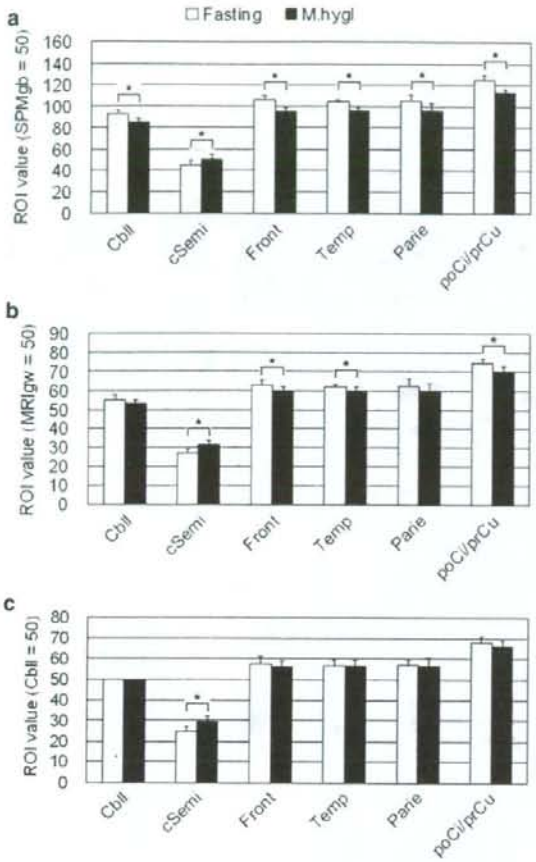

Fig. 4 Relative regional FDG uptake in the brain in the fasting and mild hyperglycemic (M.hygl) conditions in the SPMgb- (**a**), MRIgw- (**b**), and Cbll- (**c**) reference-based images. *Cbll* cerebellar cortex, *cSemi* centrum semiovale, *Front* frontal cortex, *Temp* temporal cortex, *Parie* parietal cortex, and *poCilprCu* posterior cingulate/precuneus. The region of interest (ROI) values are shown as mean and SD ($n = 9$). *$P < 0.05$ (paired Wilcoxon t test with Bonferroni correction)

The most notable factor making a difference in the SPM results (T values) depending on the reference regions would be the difference in the relative amount of gray matter included in each reference region (Fig. 1). This is because the FDG uptake alterations induced by mild hyperglycemia in the gray matter and other regions were toward opposite directions: a decrease in the gray matter, but an increase in the white matter and extracerebral tissues (Figs. 3, 4).

Regarding the test–retest reproducibility of FDG-PET, several groups have confirmed that the global CMRglc and rCMRglc were reproducible, and the relative rCMRglc was more stable than the rCMRglc in the fasting condition within and among normal subjects with ages ranging from 23 years to 38 years in an ROI-based analysis [15–18]. Prior to the present study, we also confirmed the reproducibility of FDG-PET in the fasting condition within and among aged healthy subjects with ages ranging from 48 years to 80 years by the same method used in the present SPM-based analysis (unpublished data). The intrasubject test was done within 10 subjects, and the intersubject test was done between the 10 subjects and 9 subjects. The paired t test for the comparison within subjects and the two-sample t test for the comparison among subjects by SPM did not reveal variations in any of the normalization processes based on SPMgb, MRIgw, or Cbll ($P < 0.001$, uncorrected; $k = 300$).

In the FDG-PET study conducted by Hasselbalch et al. [6], the plasma glucose level (270 mg/dl) during hyperglycemia was approximately twice as high as that observed in the mild hyperglycemic condition (137 mg/dl) of the present study. In addition, the plasma glucose levels in their study were clamped by a constant infusion of somatostatin and insulin and variable intravenous infusions of 20% glucose. In terms of the glucose intake method, extrinsic factors of the brain (intravenous and passive intake of nutrients) were reflected in their study, but intrinsic factors (oral and spontaneous intake of nutrients) were reflected in our study. They reported that no global or regional difference in CMRglc was apparent during hyperglycemia, except for a significant increase in white matter in the centrum semiovale (42%). It is noted that Hasselbalch et al. [6] compared the quantitative CMRglc values in normal and hyperglycemic conditions, whereas we studied differences in distribution patterns by the SMP- and ROI-based analyses using relative data (Figs. 3, 4, 5). When we calculated the relative rCMRglc values normalized by the global CMRglc using the values reported in their article, the percentage rates of the relative decrease were 7.4% in the frontal cortex, 4.1% in the temporal cortex, and 8.4% in the parietal cortex, and the rate of the relative increase was calculated to be 30.6% in the centrum semiovale. It is speculated that their high glucose level induced much higher uptake in the centrum semiovale as compared with the present study: 30.6% versus 20.1% (Cbll-reference-based study, Fig. 4c). As the reason why they found no regional difference in rCMRglc values except for the significant increase in the centrum semiovale, we suspect that they compared quantitative CMRglc values between two conditions using ROI-based analysis. It would be of great interest if the paired t test of SPM using their CMRglc data provided results similar to ours in Fig. 3.

The following possible reasons can explain the phenomenon that FDG distribution patterns in the brain

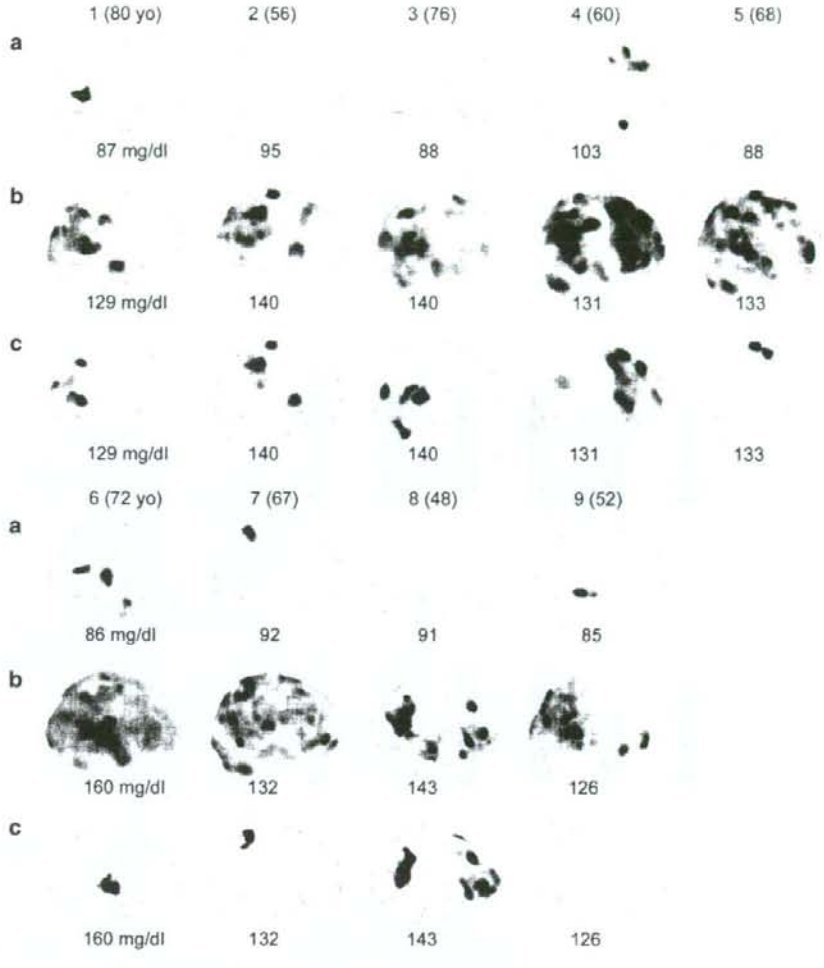

Fig. 5 SPM "Compare-populations: 1 scan/subject (Ancova)" with age as a covariate between each scan of the 9 subjects in the fasting or mild hyperglycemic condition and the scans of the other 18 of the 19 subjects in the fasting condition ($P < 0.01$, uncorrected, $k = 300$): "uptake of one scan in Fasting < uptake of the normal database" in SPMgb-reference-based analysis (**a**), and "uptake of one scan in M.hygl < uptake of the normal database" in SPMgb-(**b**) and MRIgw-reference-based analyses (**c**). No decreased uptake patterns in any subjects were revealed in Cbll-reference-based analysis (not shown). Subject numbers and ages in *parentheses* are presented on the top of three images of each subject and plasma glucose concentration (average) is presented at the bottom of each image

were regionally altered in the fasting and mild hyperglycemic conditions. (1) Difference in the cytoarchitecture that may cause a regional difference in the expression of glucose transporters and hexokinase and in turn may cause a regional difference in the lumped constant [5, 19, 20]. (2) The influence of the endocrine system, autonomic nervous system, psychological factors, or plasma glucose level related to the dietary condition may affect the regional cerebral function [6, 21, 22]. Regarding reason (1), the glucose transporter subtype 1 (GLUT1) is ubiquitously expressed in the brain, and the blood–brain barrier is a major site of its expression [23, 24]; on the other hand, the glucose transporter subtype 3 (GLUT3)—the predominant neuronal glucose transporter—is expressed in neurons [24, 25]. Asano et al. [26] had expressed the GLUT3 protein in Chinese hamster ovary (CHO) cells by the transfection of its cDNA by using an expression vector and compared its characteristics with those of the GLUT1 protein. A kinetic analysis revealed that the Michaelis constant (K_m) value of the GLUT3 protein for 3-*O*-methylglucose uptake in CHO cells was approximately 35% of that of GLUT1, whereas the K_m value of the GLUT3 protein for 2-deoxyglucose uptake was very similar to that of the GLUT1 protein. These data suggest the possibility that the regional differences in the expression ratios of GLUT1 and GLUT3 [27] and the heterogeneity of these transporters affect the FDG distribution patterns under mild hyperglycemia.

An epidemiological survey in Japan demonstrated that the frequency of diabetes mellitus diagnosed by the glucose tolerance test increased with age, with the frequency reaching 10–15% in elderly people aged 60 years or older with a high incidence of dementia [28]. In our institute these subjects sometimes undergo FDG-

PET for elucidating suspicious dementia, but the mild hyperglycemia makes it difficult to interpret the study properly. As a trial, we performed SPM "Compare-populations: 1 scan/subject (Ancova)" with age as a covariate between the FDG-PET scan of a 76-year-old subject with diabetes mellitus (plasma glucose 145 mg/dl) and mild cognitive impairment, and the 19 normal scans of the present study in SPMgb-, MRIgw-, and Cbll-reference-based analyses (unpublished data). We observed FDG distribution patterns that suggest Alzheimer's disease in the contrast "uptake of the patient < uptake of the normal database" in all reference-based analyses, but increase in the white matter in the contrast "uptake of the patient > uptake of the normal database" was not revealed in any reference-based analyses. The patient was then diagnosed with early Alzheimer's disease.

In conclusion, in the mild hyperglycemic condition, FDG uptake in the SPMgb, MRIgw, and Cbll regions was significantly decreased to 42.7%, 41.3%, and 40.0% of that in the fasting condition. It is noteworthy that FDG distribution patterns in SPMgb- (SPM default) and MRIgw-reference-based analyses were altered under mild hyperglycemia, and the decreased uptake patterns were fairly similar to those observed in Alzheimer's disease. However, when we adopted Cbll as the reference region, the decreased uptake patterns disappeared. We can recommend Cbll-reference-based analysis in the mild hyperglycemic condition to detect decreased uptake patterns. We should pay special attention to controlling the diet condition, monitoring hyperglycemia, and optimizing the reference region in SPM analysis, particularly in the diagnosis of early Alzheimer's disease in clinical FDG-PET.

Acknowledgments The authors are grateful to Drs. Hidenao Fukuyama, Kazuo Hashikawa, and Koichi Ishizu of Kyoto University for proper advice. We thank Drs. Kazunori Kawamura and Takashi Oda for the preparation of FDG and Ms. Miyoko Ando and Ms. Hiroko Tsukinari for nursing. We also thank Dr. Laurence Court for proofreading this manuscript. This research was partially supported by the Grants for Comprehensive Research Project on Longevity Science from the Ministry of Health, Labour and Welfare, Japan.

References

1. Vander Borght T, Laloux P, Maes A, Salmon E, Goethals I, Goldman S. Guidelines for brain radionuclide imaging: perfusion single photon computed tomography (SPECT) using Tc-99m radiopharmaceuticals and brain metabolism positron emission tomography (PET) using F-18 fluorodeoxyglucose. Acta Neurol Belg 2001;101:196–209.
2. Bartenstein P, Asenbaum S, Catafau A, Halldin C, Pilowski L, Pupi K, et al. European Association of Nuclear Medicine procedure guidelines for brain imaging using [^{18}F]FDG. Eur J Nucl Med Mol Imaging 2002;29:43–8.
3. Signorini M, Paulesu E, Friston K, Perani D, Colleluori A, Lucignani G, et al. Rapid assessment of regional cerebral metabolic abnormalities in single subjects with quantitative and nonquantitative [^{18}F]FDG PET: a clinical validation of statistical parametric mapping. Neuroimage 1999;9:63–80.
4. Minoshima S, Frey KA, Koeppe RA, Foster NL, Kuhl DE. A diagnostic approach in Alzheimer's disease using three-dimensional stereotactic surface projections of fluorine-18-FDG PET. J Nucl Med 1995;36:1238–48.
5. Sokoloff L, Reivich M, Kennedy C, Des Rosiers MH, Patlak CS, Pettigrew KD, et al. The [^{14}C]deoxyglucose method for the measurement of local cerebral glucose utilization: theory, procedure, and normal values in the conscious and anesthetized albino rat. J Neurochem 1977;28:897–916.
6. Hasselbalch SG, Knudsen GM, Capaldo B, Postiglione A, Paulson OB. Blood–brain barrier transport and brain metabolism of glucose during acute hyperglycemia in humans. J Clin Endocrinol Metab 2001;86:1986–90.
7. Meyer JH, Gunn RN, Myers R, Grasby PM. Assessment of spatial normalization of PET ligand images using-specific templates. Neuroimage 1999;9:545–53.
8. Benson DF, Kuhl DE, Hawkins RA, Phelps ME, Cummings JL, Tsai SY. The fluorodeoxyglucose 18F scan in Alzheimer's disease and multi-infarct dementia. Arch Neurol 1983;40:711–4.
9. Friedland RP, Brun A, Budinger TF. Pathological and positron emission tomographic correlations in Alzheimer's disease. Lancet 1985;1:228.
10. Duara R, Grady C, Haxby J, Sundaram M, Cutler NR, Heston L, et al. Positron emission tomography in Alzheimer's disease. Neurology 1986;36:879–87.
11. Rapoport SI, Horwitz B, Grady CL, Haxby JV, DeCarli C, Schapiro MB. Abnormal brain glucose metabolism in Alzheimer's disease, as measured by position emission tomography. Adv Exp Med Biol 1991;291:231–48.
12. Fukuyama H, Ogawa M, Yamauchi H, Yamaguchi S, Kimura J, Yonekura Y, et al. Altered cerebral energy metabolism in Alzheimer's disease: a PET study. J Nucl Med 1994;35:1–6.
13. Minoshima S, Foster NL, Kuhl DE. Posterior cingulate cortex in Alzheimer's disease. Lancet 1994;344:895.
14. Minoshima S, Giordani B, Berent S, Frey KA, Foster NL, Kuhl DE. Metabolic reduction in the posterior cingulate cortex in very early Alzheimer's disease. Ann Neurol 1997;42:85–94.
15. Bartlett EJ, Brodie JD, Wolf AP, Christman DR, Laska E, Meissner M. Reproducibility of cerebral glucose metabolic measurements in resting human subjects. J Cereb Blood Flow Metab 1988;8:502–12.
16. Maquet P, Dive D, Salmon E, von Frenckel R, Franck G. Reproducibility of cerebral glucose utilization measured by PET and the [^{18}F]-2-fluoro-2-deoxy-D-glucose method in resting, healthy human subjects. Eur J Nucl Med 1990;16:267–73.
17. Wang GJ, Volkow ND, Overall J, Hitzemann RJ, Pappas N, Pascani K, et al. Reproducibility of regional brain metabolic responses to lorazepam. J Nucl Med 1996;37:1609–13.
18. Tyler JL, Strother SC, Zatorre RJ, Alivisatos B, Worsley KJ, Diksic M, et al. Stability of regional cerebral glucose metabolism in the normal brain measured by positron emission tomography. J Nucl Med 1988;29:631–42.
19. Phelps ME, Huang SC, Hoffman EJ, Selin C, Sokoloff L, Kuhl DE. Tomographic measurement of local cerebral glucose metabolic rate in humans with (F-18)2-fluoro-2-deoxy-D-glucose: validation of method. Ann Neurol 1979;6:371–88.

20. Reivich M, Alavi A, Wolf A, Fowler J, Russell J, Arnett C, et al. Glucose metabolic rate kinetic model parameter determination in humans: the lumped constants and rate constants for [^{18}F]fluorodeoxyglucose and [^{11}C]deoxyglucose. J Cereb Blood Flow Metab 1985;5:179–92.
21. Tataranni PA, Gautier JF, Chen K, Uecker A, Bandy D, Salbe AD, et al. Neuroanatomical correlates of hunger and satiation in humans using positron emission tomography. Proc Natl Acad Sci USA 1999;96:4569–74.
22. Routh VH. Glucose-sensing neurons: are they physiologically relevant? Physiol Behav 2002;76:403–13.
23. Pardridge WM, Boado RJ, Farrell CR. Brain-type glucose transporter (GLUT-1) is selectively localized to the blood–brain barrier: studies with quantitative western blotting and in situ hybridization. J Biol Chem 1990;265:18035–40.
24. Maher F, Vannucci SJ, Simpson IA. Glucose transporter proteins in brain. FASEB J 1994;8:1003–11.
25. Nagamatsu S, Sawa H, Kamada K, Nakamichi Y, Yoshimoto K, Hoshino T. Neuron-specific glucose transporter (NSGT): CNS distribution of GLUT3 rat glucose transporter (RGT3) in rat central neurons. FEBS Lett 1993;334:289–95.
26. Asano T, Katagiri H, Takata K, Tsukuda K, Lin JL, Ishihara H, et al. Characterization of GLUT3 protein expressed in Chinese hamster ovary cells. Biochem J 1992;288:189–93.
27. Yano H, Seino Y, Inagaki N, Hinokio Y, Yamamoto T, Yasuda K, et al. Tissue distribution and species difference of the brain type glucose transporter (GLUT3). Biochem Biophys Res Commun 1991;174:470–7.
28. Ito H. The summary of "Treatment guidelines of diabetes mellitus in the elderly people" drafted by a group of comprehensive research on aging and health (in Japanese). Geriatric Med 1996;34:899–902.

Ann Nucl Med (2008) 22:143–146
DOI 10.1007/s12149-007-0088-x

TECHNICAL NOTE

Shortened protocol in practical [^{11}C]SA4503-PET studies for sigma$_1$ receptor quantification

**Muneyuki Sakata · Yuichi Kimura · Mika Naganawa
Masatomo Ishikawa · Keiichi Oda · Kenji Ishii
Kenji Hashimoto · Kunihiro Chihara · Kiichi Ishiwata**

Received: 23 April 2007 / Accepted: 9 October 2007
© The Japanese Society of Nuclear Medicine 2008

Abstract In practical positron emission tomography (PET) diagnosis, a shortened protocol is preferred for patients with brain disorders. In this study, the applicability of a shortened protocol as an alternative to the 90-min PET scan with [^{11}C]SA4503 for quantitative sigma$_1$ receptor measurement was investigated. Tissue time–activity curves of 288 regions of interest in the brain from 32 [^{11}C]SA4503-PET scans of 16 healthy subjects prior to and following administration of a selective serotonin reuptake inhibitor (fluvoxamine or paroxetine) were applied to two algorithms of quantitative analysis: binding potential (BP) was derived from compartmental analysis based on nonlinear estimation, and total distribution volume (tDV) was derived from Logan plot analysis. As a result, although both BP and tDV tended to be underestimated by the shortened method, the estimates from the shortened protocol had good linear relationships with those of the full-length protocol. In conclusion, if approximately 10% differences in the estimated results are acceptable for a specific purpose, then a 60-min measurement protocol is capable of providing reliable results.

Keywords [^{11}C]SA4503 · Sigma$_1$ receptor · PET · Kinetic

M. Sakata · Y. Kimura · M. Ishikawa · K. Oda · K. Ishii · K. Ishiwata
Positron Medical Center, Tokyo Metropolitan Institute of Gerontology, Tokyo, Japan

M. Sakata · K. Chihara
Graduate School of Information Science, Nara Institute of Science and Technology, Nara, Japan

Y. Kimura (✉) · M. Naganawa
Image Analysis Team, Biophysics Group, Molecular Imaging Center, National Institute of Radiological Sciences, 4-9-1 Anagawa, Inage-ku, Chiba 263-8555, Japan
e-mail: ukimura@ieee.org

M. Naganawa
Japan Society for the Promotion of Science, Tokyo, Japan

M. Ishikawa
Department of Psychiatry, Chiba University, Chiba, Japan

K. Hashimoto
Division of Clinical Neuroscience, Chiba University Center for Forensic Mental Health, Chiba, Japan

Introduction

The aim of this study was to offer a quantitative measure to decide the adoption of a shortened protocol with clinical consideration in positron emission tomography (PET) studies using [^{11}C]SA4503 for quantitative sigma$_1$ receptor measurement. The [^{11}C]SA4503 is a specific radioligand for mapping sigma$_1$ receptors [1, 2], which play a role as modulators of signal transduction in the human brain. The development of new sigma receptor ligands enables the observation of pathophysiological backgrounds of cerebral degenerative diseases and the effects of therapeutic treatment of neuropsychiatric diseases; for example, the clinical application of [^{11}C]SA4503-PET to patients with Parkinson's disease and to a receptor occupancy study on haloperidol have been already reported [3, 4].

For quantitative measurement, a 90-min dynamic scan is required to estimate the kinetics of [^{11}C]SA4503 [5]. However, from a clinical point of view, a shortened protocol is preferred for patients with brain disorders. In general, a long dynamic scan is difficult to perform

on patients with psychosomatic disorders or dementia, and sometimes causes a loss of image quality because of abrupt body movement or abortion of the PET scan. Therefore, in this study, shortened protocols for the PET measurement were investigated using the dynamic data of 90-min PET scans, and the influences on the [^{11}C]SA4503-sigma$_1$ receptor binding were studied both for compartmental analysis based on nonlinear estimation and for Logan plot analysis.

Materials and methods

Sixteen normal male volunteers (age 35 ± 4 years) were recruited. All subjects underwent two PET scans with [^{11}C]SA4503 before and 4–4.5 h after the administration of one of the two serotonin reuptake inhibitors; 12 subjects were administered fluvoxamine (50, 100, 150, or 200 mg, $n = 3$ for each) having moderate affinity for the sigma$_1$ receptors, and the others were administered paroxetine (20 mg) with negligible affinity. All study protocols were approved by the Ethics Committee of the Tokyo Metropolitan Institute of Gerontology and the Ethics Committee of Chiba University Graduate School of Medicine, and informed consent was given by all subjects. According to the method described earlier [2], the 90-min PET scans were performed dynamically using SET-2400W (Shimadzu, Kyoto, Japan) in 2D mode (10 s × 6 frames, 30 s × 3 frames, 60 s × 5 frames, 150 s × 5 frames, and 300 s × 14 frames), with arterial blood sampling (10 s, 20 s, 30 s, 40 s, 50 s, 60 s, 70 s, 80 s, 90 s, 100 s, 110 s, 120 s, 135 s, and 150 s and 3 min, 5 min, 7 min, 10 min, 15 min, 20 min, 30 min, 40 min, 50 min, 60 min, 75 min, and 90 min) with metabolite correction (3 min, 10 min, 20 min, 30 min, 40 min, and 60 min). The injected dosages [mean ± standard deviation (SD)] and the specific activity were 704 MBq ± 145 MBq/11.3 nmol ± 6.6 nmol and 80.0 TBq/mmol ± 40.5 TBq/mmol, respectively.

Regions of interest (ROIs) were placed on the frontal, temporal, parietal, and occipital cortices, caudate, putamen, thalamus, anterior cingulated gyrus, and cerebellar hemispheres, and the averaged tissue time–activity curves (tTACs) were applied to a model estimation process for 288 ROIs (9 ROIs × 16 patients × 2 PET scans before and after the administration of a serotonin reuptake inhibitor).

Two algorithms of quantitative analysis were applied as the model estimation. First, a two-tissue three-compartment model was fitted on the tTAC using a nonlinear estimation algorithm as described earlier [2], and the rate constants of K_1 to k_4 were derived. Binding potential (BP) was calculated from the rate constants as k_3/k_4. Second, the total distribution volume (tDV) was estimated by Logan plot analysis [6]. The applicability of the compartmental model and the Logan plot for the kinetic analysis of [^{11}C]SA4503 has been validated earlier [2]. In this study, five different durations were used in the protocols investigated. They corresponded to dynamic 40-min, 50-min, 60-min, 75-min, and 90-min PET scans following the administration of [^{11}C]SA4503, and the BPs for each period were calculated and designated as BP_{60}, BP_{90}, and so on. For the Logan plot analyses, the starting time used was 20 min or 30 min after tracer administration and the end times were 40 min, 50 min, 60 min, 75 min, and 90 min. The values were denoted as $tDV_{20\text{-}60}$, $tDV_{30\text{-}90}$, and so on. According to an earlier report [2], BP_{90} and $tDV_{30\text{-}90}$ were used as the standards, and the changes in the estimated BPs and tDVs were examined.

Results and discussion

All nonlinear estimations of BP were well converged, and all Logan plots were suitable for the estimation of tDV except for $tDV_{30\text{-}40}$. The relationship between the standard BP_{90} and $tDV_{30\text{-}90}$ and the corresponding estimate in the shortened protocol was evaluated. In the case of the 60-min protocol, as shown in Fig. 1, 7% and 10% underestimations were observed for BP and tDV, respectively. However, good linear relationships were observed for both BP and tDV. As shown in Fig. 2, in the 60-min protocol, the means of the absolute differences from the standard estimates in BP and tDV were 11.5%, 9.3%, and 10.0% for BP_{60}, $tDV_{30\text{-}60}$, and $tDV_{20\text{-}60}$, respectively. The differences decreased to 8.7%, 7.7%, and 7.0% after the corrections using the correlation equations shown in Fig. 1. Even in the 40-min protocol, those means are less than 20% if the data from 20 min were used for the Logan plot. The SD of the absolute difference increased according to the shortening of the duration. In Table 1, the estimated values for the mean and coefficient of variation (CV) of the BPs and the tDVs in the 90-min, 60-min, and 40-min protocols are summarized. Although the estimated BPs and tDVs were underestimated owing to the shortened scan, the changes in the CV were acceptably small. Usually, the Logan plot, which was implemented from a linear estimation, should be more stable than the nonlinear estimation; however, in the present shortened protocol, the results were approximately equivalent as fewer data points were utilized for the Logan plot. It is noted that tDV included free and specifically/nonspecifically bound ligands, but that in the case of [^{11}C]SA4503, tDV has a good linear relationship with BP [7].

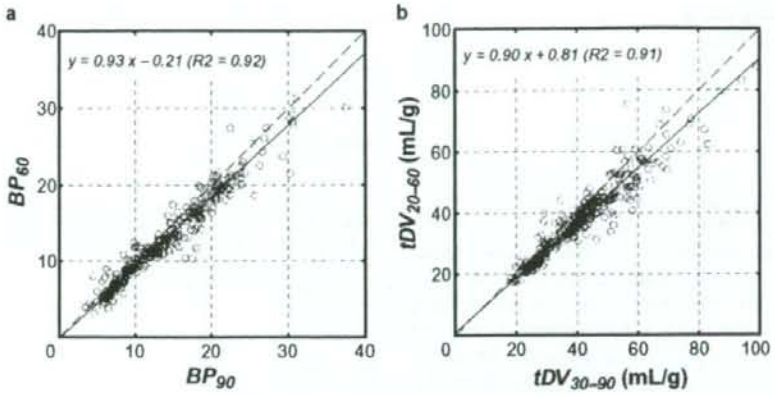

Fig. 1 Relationship of binding parameters of [^{11}C]SA4503 between the estimates in the standard 90-min protocol and those in the shortened protocol. **a** BP_{90} and BP_{60} are binding potentials (BPs) of 90-min and 60-min protocols, respectively, derived from the compartmental analysis based on nonlinear estimation. **b** $tDV_{30\text{-}90}$ and $tDV_{20\text{-}60}$ are total distribution volumes (tDVs) derived from the Logan plot analysis using 30–90-min and 20–60-min data, respectively. In each panel, the *solid line* indicates the regression line and the *dashed line* indicates $y = x$

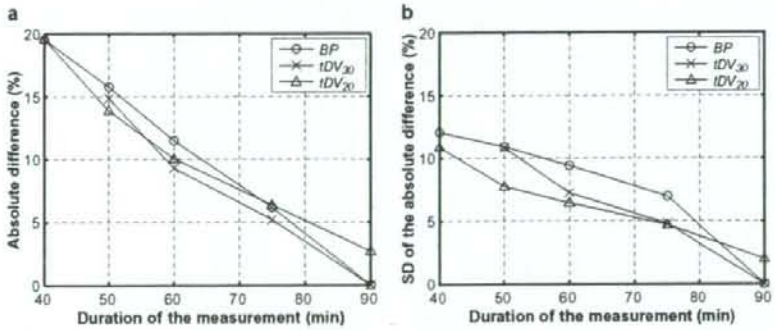

Fig. 2 Mean (**a**) and standard deviation (**b**) of the absolute differences between the binding parameters of [^{11}C]SA4503 in the standard protocol and those in the shortened protocol. In the standard protocol, the BP was derived from a nonlinear estimation using whole 90-min data and the tDV from a Logan plot using the data recorded from 30 min to 90 min. *Circle*, BP and *cross*, tDV_{30} derived using the data from 30 min after the injection of [^{11}C]SA4503 to the end of the protocol, and *triangle*, tDV_{20} derived using the data from 20 min to end

Table 1 Estimated total distribution volumes and binding potentials (mean ± CV, $n = 32$)

	BP_{90}	BP_{60}	BP_{40}	$tDV_{30\text{-}90}$ (ml/g)	$tDV_{20\text{-}60}$ (ml/g)	$tDV_{20\text{-}40}$ (ml/g)
Frontal cortex	13.2 ± 0.4	12.2 ± 0.4	11.4 ± 0.4	39.8 ± 0.3	36.2 ± 0.3	33.2 ± 0.3
Temporal cortex	16.8 ± 0.4	15.5 ± 0.4	13.8 ± 0.4	41.6 ± 0.3	38.5 ± 0.3	36.2 ± 0.4
Parietal cortex	13.2 ± 0.4	12.0 ± 0.4	11.1 ± 0.4	38.5 ± 0.3	35.0 ± 0.3	32.1 ± 0.4
Occipital cortex	12.4 ± 0.5	11.2 ± 0.4	10.1 ± 0.4	38.8 ± 0.3	35.1 ± 0.3	32.2 ± 0.3
Caudate	11.8 ± 0.4	11.7 ± 0.5	10.3 ± 0.5	33.4 ± 0.2	32.1 ± 0.3	27.5 ± 0.3
Putamen	12.3 ± 0.4	11.3 ± 0.4	11.1 ± 0.4	39.0 ± 0.3	34.8 ± 0.3	29.8 ± 0.2
Thalamus	13.0 ± 0.4	11.5 ± 0.4	10.4 ± 0.4	43.6 ± 0.2	39.9 ± 0.3	36.7 ± 0.4
Anterior cingulated gyrus	15.1 ± 0.4	13.9 ± 0.4	12.9 ± 0.4	42.2 ± 0.3	39.5 ± 0.3	34.7 ± 0.4
Cerebellar hemisphere	19.2 ± 0.4	17.3 ± 0.4	15.6 ± 0.5	55.7 ± 0.4	49.8 ± 0.4	46.2 ± 0.4

For developing simplified methods of [^{11}C]SA4503-PET for routine clinical studies, we investigated the shortened protocol in this study, but neither static imaging nor the kinetic analysis is based on the reference-tissue model. The reason is that [^{11}C]SA4503 does not always reach a pseudo-equilibrium state between free and receptor-bound radioligands during a 90-min PET scan because of its relatively high affinity for sigma$_1$ receptors. As another reason, no reference region being devoid of sigma$_1$ receptors is available because sigma$_1$ receptors are present in all brain regions. Earlier we have investigated whether the white matter can be used as a reference region because it is considered that the number of neuroreceptors is negligible in it. However, BP values estimated from the Logan plot analysis based on the reference (white matter)-tissue model were not correlated with those calculated from a two-tissue three-compartment model.

In the present study, we used the data set for two PET scans of 16 healthy subjects before and after administration of one of the two selective serotonin reuptake inhibitors. Because the density of many neuroreceptors is usually decreased in brain disorders, the shortened protocol should be applicable to measuring the decreased as well as normal densities of the sigma$_1$ receptors. The partial blockade of sigma$_1$ receptors by selective serotonin reuptake inhibitors corresponds to the decreased density of sigma receptors in the brain. Earlier we confirmed that by administering fluvoxamine, sigma$_1$ receptors were dose-dependently occupied by fluvoxamine up to approximately 60% [8]; that is, the densities of sigma$_1$ receptors were apparently reduced by 40% at the most. Therefore, good linear relationships between the shortened protocol and the full-length protocol over a wide range of receptors densities mean that the shortened protocol could be applicable to subjects whose densities of sigma$_1$ receptors are lowered.

Considering the results, approximately 10% absolute differences occurred in BP_{60}, $tDV_{30\text{-}60}$, and $tDV_{20\text{-}60}$, respectively, if a 60-min shortened protocol was adopted. The differences slightly decreased to 7%–9% after the corrections using the correlation equations shown in Fig. 1. Therefore, if the differences of the estimated results are acceptable for a specific purpose of the experiment, a 60-min measurement protocol would be capable of providing reliable results in [^{11}C]SA4503-PET.

Acknowledgments This work was supported in part by the Grant-in-Aid for the 21st Century COE from the Ministry of Education, Culture, Sports, Science and Technology of Japan (MS and KC), by the Grant-in-Aid for Scientific Research (C), No. 18591373, 2006 and 2007 from the Japan Society for the Promotion of Science (YK), and by the Program for Promotion of Fundamental Studies in Health Sciences of the National Institute of Biomedical Innovation, Japan (No: 06-46, KH and KI).

References

1. Kawamura K, Ishiwata K, Tajima H, Ishii S, Matsuno K, Homma Y, et al. In vivo evaluation of [^{11}C]SA4503 as a PET ligand for mapping CNS sigma$_1$ receptors. Nucl Med Biol 2000;27:255–61.
2. Sakata M, Kimura Y, Naganawa M, Oda K, Ishii K, Chihara K, et al. Mapping of human cerebral sigma$_1$ receptors using positron emission tomography and [^{11}C]SA4503. Neuroimage 2007;35:1–8.
3. Mishina M, Ishiwata K, Ishii K, Kitamura S, Kimura Y, Kawamura K, et al. Function of sigma$_1$ receptors in Parkinson's disease. Acta Neurol Scand 2005;112:103–7.
4. Ishiwata K, Oda K, Sakata M, Kimura Y, Kawamura K, Oda K, et al. A feasible study of [^{11}C]SA4503-PET for evaluating sigma$_1$ receptor occupancy by neuroleptics: the binding of haloperidol to sigma$_1$ and dopamine D_2-like receptors. Ann Nucl Med 2006;20:569–73.
5. Watabe H, Ikoma Y, Kimura Y, Naganawa M, Shidahara M. PET kinetic analysis: compartmental model. Ann Nucl Med 2006;20:583–8.
6. Logan J, Fower JS, Volkow ND, Wolf AP, Dewey SL, Schlyer DJ, et al. Graphical analysis of reversible radioligand binding from time–activity measurements applied to [N-^{11}C-methyl]-(–)-cocaine PET studies in human subjects. J Cereb Blood Flow Metab 1990;10:740–7.
7. Kimura Y, Naganawa M, Sakata M, Ishikawa M, Mishina M, Oda K, et al. Distribution volume as an alternative to the binding potential for sigma$_1$ receptor imaging. Ann Nucl Med 2007;21:533–5.
8. Ishikawa M, Ishiwata K, Ishii K, Kimura Y, Sakata M, Naganawa M, et al. High occupancy of sigma-1 receptors in the human brain after single oral administration of fluvoxamine: a PET study using [^{11}C]SA4503. Biol Psychiatry 2007;62:878–83.